Low-Frequency Phonon Modes and Negative Thermal Expansion in $A(MO_4)_2$ (A = Zr, Hf and M = W, Mo) by Raman and Terahertz Time-Domain Spectroscopy

E. J. Liang,*,† Yuan Liang,†,‡ Yan Zhao,§ Jie Liu,§ and Yijian Jiang§

School of Physical Science & Engineering and Key Laboratory of Materials Physics of Ministry of Education of China, Zhenghou University, Zhengzhou 450052, China, Department of Physics, Fudan University, Shanghai 200433, China, and Institute of Laser Engineering, Beijing University of Technology, Beijing, 100124, China

Received: June 15, 2008; Revised Manuscript Received: September 21, 2008

The low-frequency phonon modes of cubic ZrW_2O_8 and HfW_2O_8, and trigonal $ZrMo_2O_8$ and $HfMo_2O_8$ have been comparatively studied by Raman and terahertz time-domain spectroscopy. It is shown that there appear a number of distinctive low-frequency modes below 150 cm^{-1} in the cubic ZrW_2O_8 and HfW_2O_8 in both Raman and terahertz spectra which are attributed to the librational and translational motions of the polyhedra whereas only one weak mode is present in the Raman but absent in the THz spectra of the trigonal $ZrMo_2O_8$ and $HfMo_2O_8$ in the same region, which is assigned to the interlayer breathing. It is found that the lowest optical phonon mode at about 40 cm^{-1} disappears accompanied by obvious weakening of the lowest asymmetric stretching mode for ZrW_2O_8 and HfW_2O_8 across the order−disorder phase transition temperature. It gives direct evidence of reduction in the number of rigid unit modes (RUMs) in the high-temperature phase. It is shown that the correlated motions of the libration and transilation of the WO_4 tetrahedra and the ZrO_6/HfO_6 octahedra with the out-of-phase asymmetric stretching of the two neighboring WO_4 tetrahedra contribute a large portion to the NTE in the low-temperature phase and some of the correlated motions may be destroyed across the order−disorder phase transition, causing a smaller negative thermal expansion in the high-temperature phase. The lack of RUMs in trigonal $ZrMo_2O_8$ and $HfMo_2O_8$ is the cause of their positive thermal expansion.

I. Introduction

Materials with negative thermal expansion (NTE) have attracted significant attention in recent years due to scientific curiosity and technological interest.[1−10] Among these materials, ZrW_2O_8 and HfW_2O_8 are of considerable interest due to their large isotropic NTE over a wide range of temperature.[2] They exhibit a framework structure that consists of the corner-sharing WO_4 tetrahedra and ZrO_6 or HfO_6 octahedra. The polyhedra in ZrW_2O_8 are connected at almost all vertices, the exception being one terminal oxygen atom in each WO_4 tetrahedron. The NTE in ZrW_2O_8 was explained in terms of the rigid unit mode (RUM) model.[3] The basic RUM model for NTE is based on the idea that rotations of linked polyhedra will pull them in toward each other; this motion will be seen more locally as the flexing of the Zr−O−W linkage through transverse motions of the O atom, without significant stretching of the Zr−O and W−O bonds.[4] These vibrations are low-frequency librational and translational modes of the undistorted polyhedra. The low-energy vibrational motion of WO_4 units brings about another interesting physical property of ZrW_2O_8 and HfW_2O_8, which undergo a structural phase transition around 440 K from an acentric (α, space group $P2_13$) to a centric structure (β, space group $pa\bar{3}$) with increasing temperature.[1,11] The structural phase transition is related to the orientation of the unshared vertex of the WO_4 unit. In the low-temperature phase, two neighboring WO_4 tetrahedra on the [1 1 1] body diagonal in the unit cell point their unshared vertexes to the [1 1 1] direction, whereas they are randomly oriented to [1 1 1] or −[1 1 1] directions in the high-temperature phase. The structural phase transition of ZrW_2O_8 and HfW_2O_8 is therefore of order−disorder type.

The phonon density of states below 300 K for ZrW_2O_8 was measured by Ernst et al.[12] from neutron scattering which show several pronounced peaks below 50 meV. They applied low-energy modes from 1.5 to 8.5 meV (12.−68.6 cm^{-1}), assumed to have equal Grüneisen parameters of −14 to interpret the negative thermal expansion. Ramirez and Kowach[13] measured the specific heat of ZrW_2O_8 from 1 to 300 K and suggested that a weakly dispersive optical mode around 5 meV (40.3 cm^{-1}) was responsible for the NTE by fitting the data with a combination of two Debye and two Einstein modes. Using this phonon distribution, David et al.[14] determined the mode Grüneisen parameters by fitting the lattice parameter data and suggested that two Einstein modes at 3.3 (26.6 cm^{-1}) and 5.8 meV (46.7 cm^{-1}) were the dominant contributors to the NTE. This is, however, different from their later conclusion that a low-energy peak around 4.7 meV (37.9 cm^{-1}) is associated with the NTE of ZrW_2O_8. Evans et al.[15] utilized two Debye modes to empirically fit their low-temperature lattice parameters and identified the mode with a characteristic Debye temperature of 95 K (65 cm^{-1}) to have a negative mode Grüneisen parameter. Yamamura et al.[16,17] measured the heat capacity of HfW_2O_8 from 80 to 330 K and determined effective phonon density of states, assuming one Debye, two Einstein, and two rectangular functions. They concluded that the two Einstein modes at 3.36 (27 cm^{-1}) and 5.51 meV (44 cm^{-1}) have mode Grüneisen parameters of −44 and −8.7,[16] conflicting to their own conclusion that the two Einstein modes are at 3.52 (28 cm^{-1}) and 9.82 meV (79 cm^{-1}) and have mode Grüneisen parameters of −40 and 0.06, respectively.[17] All these studies were focused on the

* Corresponding Author: ejliang@zzu.edu.cn.
† Zhenghou University.
‡ Fudan University.
§ Beijing University of Technology.

10.1021/jp805256d CCC: $40.75
Published on Web 11/14/2008

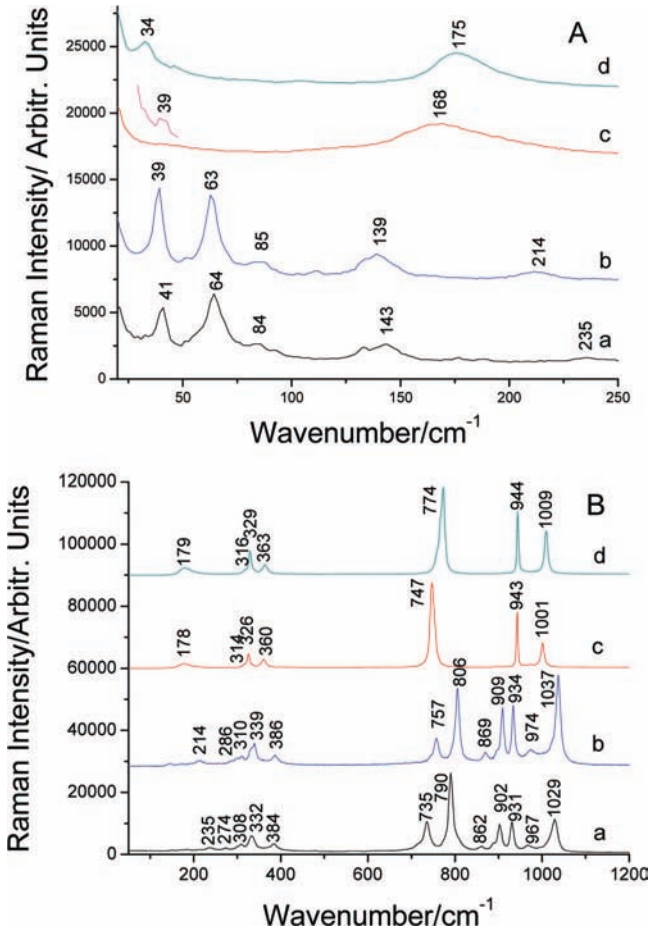

Figure 1. Raman spectra of (a) α-ZrW_2O_8, (b) α-HfW_2O_8, (c) α-$ZrMo_2O_8$, and (d) α-$HfMo_2O_8$ in (A) low- and (B) high-frequency regions.

low-temperature phase and the interpretation of the NTE based on heat capacity or specific heat measurements relies on the types of functions and the number of each function selected in fitting the data. Although Raman spectroscopy has been used to study the phase transition, phonon characters, and the mechanism of NTE in ZrW_2O_8 and HfW_2O_8,[11,17−27] most of the studies were focused on the low-temperature and high-pressure phases. The expansion is still negative in the high-temperature phase but smaller in magnitude, presumably because the disordered structure reduces the number of RUMs. However, no direct evidence on the reduction of the number of RUMs has been reported. Besides, the order−disorder phase transition was revealed by calorimetric and X-ray diffraction studies,[28,29] but not closely studied by Raman spectroscopy.[11,17−27] In this paper, we study the Raman spectra of cubic ZrW_2O_8 and HfW_2O_8 at room temperature as well as across their phase transition temperature and compare them with those of the trigonal $ZrMo_2O_8$ and $HfMo_2O_8$ which have positive thermal expansion, with the aim to understand the effect of the replacement of Zr by Hf on the vibrational properties and the difference in the NTE in the low- and high-temperature phases of cubic ZrW_2O_8 and HfW_2O_8. The low-frequency phonon modes of the four samples are also studied by THz time-domain spectroscopy (THz-TDS). The trigonal $ZrMo_2O_8$ or $HfMo_2O_8$ has a two-dimensional (2D) network structure with layers perpendicular to the *c* axis, which are formed from the ZrO_6 octahedra linked together by MoO_4 tetrahedra. Three of the four oxygen atoms of the molybdate tetrahedra are linked to different Zr atoms. The fourth oxygen atom of each tetrahedron points into the interlayer region and the oxygen atoms form a cubic-close-packed anion arrangement.[30,31] The layers are bonded together by van der Waals forces.

II. Experimental Section

The samples of ZrW_2O_8, HfW_2O_8, $ZrMo_2O_8$, and $HfMo_2O_8$ were prepared by solid state reactions and characterized by X-ray diffraction (XRD) and Raman spectroscopy. A Renishaw MR-2000 Raman spectrometer with 532 nm laser wavelengths excitation and a Jobin-Yvon T64000 Raman spectrometer with 514.5 nm laser wavelength excitation were used for Raman spectroscopic studies. XRD measurements were carried out with a D/Max-2550 PC X-Ray Diffractometer from Rigaku Corporation (Japan). Samples were mixed with polyethylene (PE) powder at a weight ratio of 3:1 and made into pellets with thickness between 0.4 and 0.6 mm by applying an approximate pressure of 22 MPa with an oil press. PE is nearly transparent under 2 THz. The THz-time domain spectra of theses samples were measured in a transmission mode with a THz-TDS system that consists of a femtosecond laser and a THz-TD spectrometer. A mode-locked Ti:sapphire laser provided pulses of 100 fs duration at a center wavelength of 800 nm with average power of 700 mW and a repetition rate of 80 MHz. The laser light is divided into two beams, a pump and a probe. The pump laser beam was illuminated on a biased GaAs photoconductor antenna to generate the THz wave. The generated THz wave was collimated and focused on the sample by a pair of parabolic mirrors. After being transmitted through the sample, this THz wave was collimated and focused again into a ZnTe electrooptic (EO) crystal by the second pair of parabolic mirrors. The probe beam is coincident with the THz wave to detect polarization changes due to Pockel's effect of THz. The linearly polarized probe beam experiences the polarization change due to a birefringence by the THz wave in the ZnTe EO crystal. With varying time delay between the THz wave and optical probe with a very small gating time step, the entire THz wave profile is traced and its waveform decoded. The spectral resolution of the setup is better than 40 GHz. The available bandwidth of the spectrometer is 0.3−2.0 THz (6−67 cm^{-1}). The whole system was placed in a closed box purged with dry nitrogen to minimize absorption by residual water vapor in the beam path.

III. Results and Discussion

XRD analysis demonstrated that ZrW_2O_8 and HfW_2O_8 crystallized in cubic (α) phase with space group $P2_13$ while $ZrMo_2O_8$ and $HfMo_2O_8$ crystallized in trigonal (α) phase with space group $P\bar{3}1c$. Parts A and B of Figure 1 show the Raman spectra of α-ZrW_2O_8, α-HfW_2O_8, α-$ZrMo_2O_8$, and α-$HfMo_2O_8$ in the low- and high-frequency region, respectively. The frequencies for a free tungstate ion are close to 930, 830, 405, and 320 cm^{-1}, respectively.[32] By comparison with the Raman spectra of the free tungstate ion, the Raman modes from 1040 to 910 cm^{-1}, from 910 to 700 cm^{-1}, from 400 to 320 cm^{-1}, and from 320 to 280 cm^{-1} were previously identified as symmetric stretching (ν_1), asymmetric stretching (ν_3), asymmetric bending (ν_4), and symmetric bending (ν_2) modes in the WO_4 tetrahedra in α-HfW_2O_8 and α-ZrW_2O_8, respectively,[11,17−27] while the other modes below 280 cm^{-1} were ascribed to the lattice modes arising from Zr or Hf atom motions and translational and librational (hindered rotation) motions of the WO_4 tetrahedra and the ZrO_6/ HfO_6 octahedra.[19] A comparison of the Raman spectra a and b of Figure 1 reveals that although α-ZrW_2O_8 and α-HfW_2O_8 have similar phonon band structures due to their structural similarity, the replacement of Zr by Hf

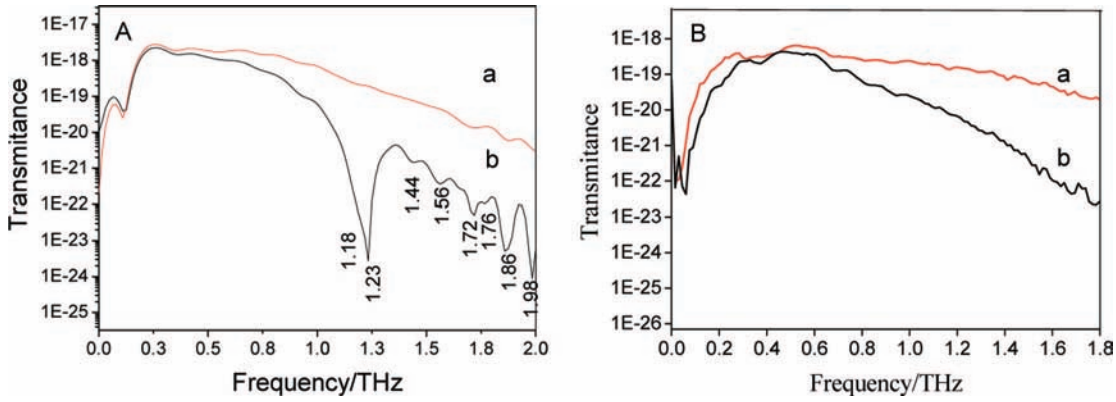

Figure 2. THz spectra of (A) α-ZrW_2O_8 and (B) α-$ZrMo_2O_8$ measured by THz time-domain spectroscopy: (a) dry nitrogen and (b) sample.

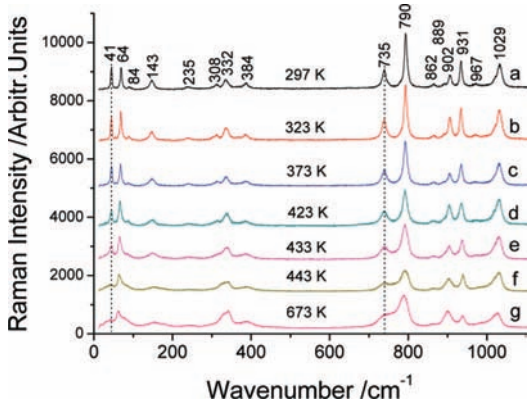

Figure 3. Raman spectra of ZrW_2O_8 at different temperatures: (a) 297, (b) 323, (c) 373, (d) 423, (e) 433, (f) 443, and (g) 673 K.

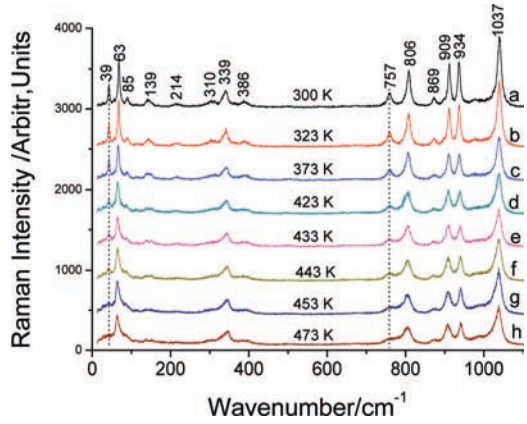

Figure 4. Raman spectra of HfW_2O_8 at different temperatures: (a) 297, (b) 323, (c) 373, (d) 423, (e) 433, (f) 443, (g) 453, and (h) 673 K.

atoms has obvious effects on the band positions and the distribution in phonon density of states. The lowest asymmetric stretching modes (735 and 790 cm^{-1}) are pushed much more to higher energies ($\Delta\omega = 22$ and 16 cm^{-1}) than the symmetric stretching modes ($\Delta\omega \leq 8$ cm^{-1}) while the bending vibrations remain almost unchanged, resulting in a larger phonon band gap and hardening of the modes in α-HfW_2O_8. The first principles calculations revealed similar band gaps between 400 and 730 cm^{-1} and the symmetric stretching vibrational modes in cubic ZrW_2O_8 and HfW_2O_8 being not lower than 950 cm^{-1} in any case.[33] Therefore, the Raman bands from 730 to 950 cm^{-1} and from 950 to 1040 cm^{-1} may be more reasonably assigned to the asymmetric and symmetric stretching vibrations of the WO_4 tetrahedra correlated by Zr/Hf atoms. Since all the phonon modes above 270 cm^{-1} show hardening when going from α-ZrW_2O_8 to α-HfW_2O_8, they can be unambiguously assigned to the internal bending modes of the WO_4 tetrahedra. Similar vibrational mode assignments can be given for α-$ZrMo_2O_8$ and α-$HfMo_2O_8$ in the same spectral region since they exhibit similar effects with replacement of Zr by Hf atoms. The relatively broad Raman modes around 235, 214, 168, and 175 cm^{-1} in α-ZrW_2O_8, α-HfW_2O_8, α-$ZrMo_2O_8$, and α-$HfMo_2O_8$, respectively, may be reasonably assigned to the lattice mode of Hf and Zr atom motions since they depend obviously on the nature of the Hf and Zr atoms. Below 150 cm^{-1}, a number of distinctive low-frequency modes appear in the cubic ZrW_2O_8 and HfW_2O_8 but absent in the trigonal $ZrMo_2O_8$ and $HfMo_2O_8$. These low-frequency modes can be attributed to the librational and translational motions of the polyhedra (the so-called RUMs) in the cubic ZrW_2O_8 and HfW_2O_8. The only weak Raman mode around 34−39 cm^{-1} in the trigonal $ZrMo_2O_8$ and $HfMo_2O_8$ is not a RUM.

We show in parts A and B of Figure 2 the THz spectra of ZrW_2O_8 and $ZrMo_2O_8$, respectively. It is shown that there appear a number of pronounced absorption peaks to the THz beam around 1.18 (39.5 cm^{-1}), 1.23 (41 cm^{-1}), 1.44 (48 cm^{-1}), 1.56 (52 cm^{-1}), 1.72 (57 cm^{-1}), 1.76 (59 cm^{-1}), 1.86 (62 cm^{-1}), and 1.98 (66 cm^{-1}) THz in α-ZrW_2O_8 and 1.13 (38 cm^{-1}), 1.18 (39.5 cm^{-1}), 1.60 (53 cm^{-1}), 1.66 (55 cm^{-1}), 1.79 (60 cm^{-1}), 1.88 (62 cm^{-1}), 1.92 (64 cm^{-1}), and 2.0 (67 cm^{-1}) THz in α-HfW_2O_8, respectively, whereas no corresponding modes appear in the trigonal $ZrMo_2O_8$ and $HfMo_2O_8$. The mode at about 39 cm^{-1} in trigonal $ZrMo_2O_8$ and $HfMo_2O_8$ observed in the Raman spectra is therefore IR inactive. Although trigonal $ZrMo_2O_8$ shows NTE in plane[34] and there may be QRUMs in the plane of the layers for this structure, the librational and translational motions of the polyhedra should be infrared active. Therefore, it may be more properly assigned to the interlayer breathing motion driven by van der Waals forces.

A comparison of the Raman spectra of the tungstates and molybdates shows that their internal modes (symmetric stretching, asymmetric stretching, symmetric bending, and asymmetric bending) appear in approximately the same frequency region and show similar phonon band gaps between the highest asymmetric bending and lowest asymmetric stretching modes due to the structural similarity of the tetrahedra and similar reduced mass of the W−O and Mo−O bonds. The difference in the internal phonon mode number observed can be explained by the different cite symmetries of the tungstate (C_{3v}) and molybdate (C_1) tetrahedra in the crystals. An analysis of the relation between the symmetric stretching phonon mode frequencies and the reduced mass suggests that the W−O bond is

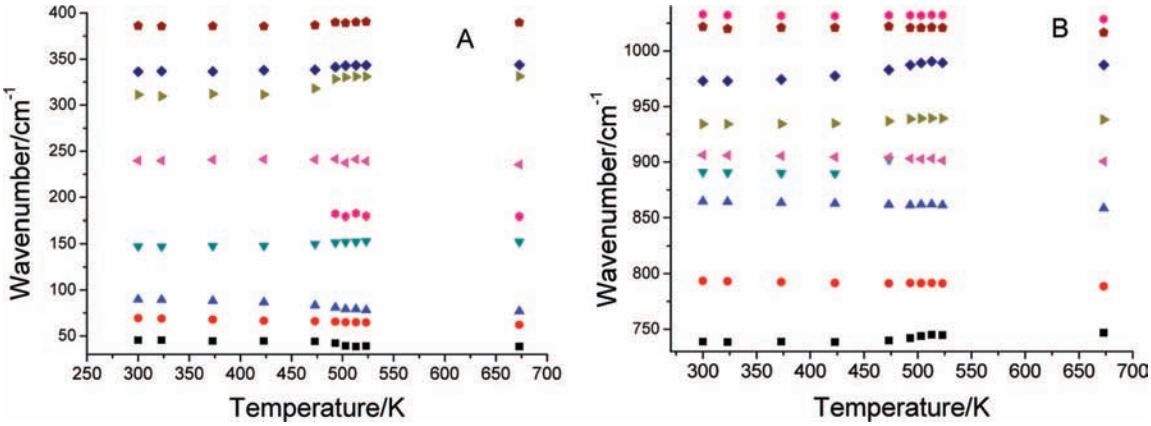

Figure 5. Temperature dependence of the Raman band positions of ZrW_2O_8.

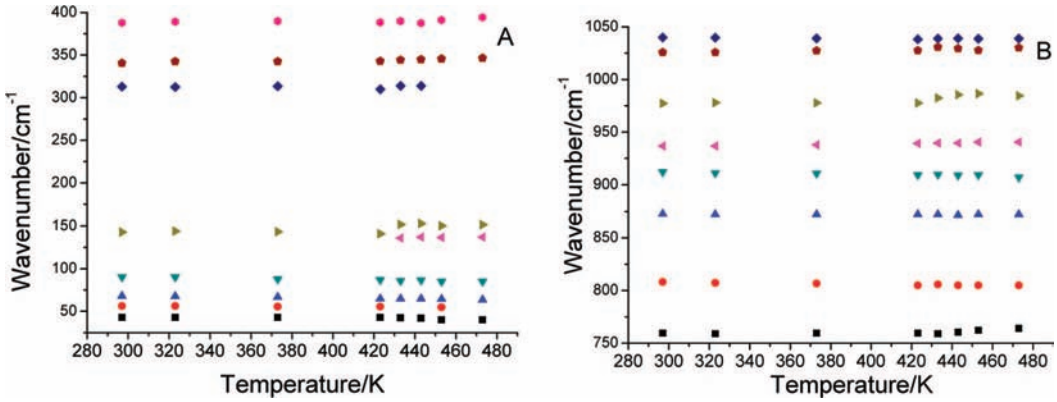

Figure 6. Temperature dependence of the Raman band positions of HfW_2O_8.

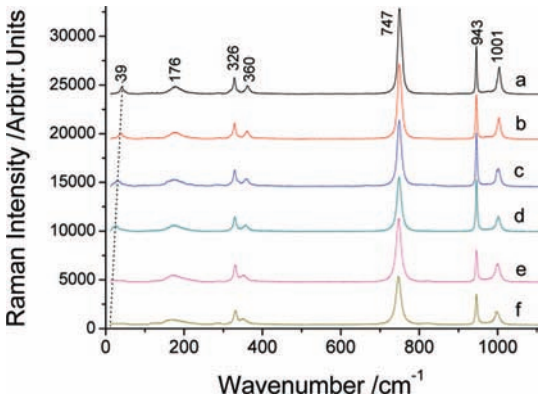

Figure 7. Raman spectra of trigonal $ZrMo_2O_8$ at different temperatures: (a) 297, (b) 323, (c) 373, (d) 413, (e) 453, and (f) 503 K.

harder than the Mo−O bonds in their corresponding tetrahedra. The lack of RUMs in trigonal $ZrMo_2O_8$ and $HfMo_2O_8$ indicates that the polyhedra in the densely packed layer do not have enough flexibility for librational and translational motions.

Figures 3 and 4 show the Raman spectra of the cubic ZrW_2O_8 and HfW_2O_8 measured at different temperatures, respectively. As expected, the Raman spectra of ZrW_2O_8 and HfW_2O_8 exhibit similar temperature behavior. While most of the Raman modes persist across the order−disorder phase transition (~440 K), the lowest Raman mode at about 40 cm^{-1} vanishes accompanied by obvious weakening of the lowest asymmetric stretching mode (~735 cm^{-1} in ZrW_2O_8 and ~757 cm^{-1} in HfW_2O_8). This presents direct evidence of reduction in the number of the RUMs in the high-temperature phase. The simultaneous change of these two modes suggests that the librational motion of the WO_4 tetrahedra and the ZrO_6/HfO_6 octahedra is more or less correlated with the out-of-phase asymmetric stretching vibrations of the two neighboring WO_4 tetrahedra in the low-temperature phase. It is inferred that such correlated motion gives rise to a large potion of contribution to the NTE in the low-temperature phase and the reduction in such contribution is the cause of smaller NTE in the high-temperature phase.

In Figures 5 and 6 we show the temperature dependence of the Raman mode positions on temperature for ZrW_2O_8 and HfW_2O_8, respectively. The linear thermal expansion coefficient α can be written in terms of the Grüneisen parameters as $\alpha = (k/3VB_0)\sum_i p_i\gamma_i(\hbar\omega_i/kT)^2 \exp(\hbar\omega_i/kT)[\exp(\hbar\omega_i/kT) - 1]^{-2}$, where V is the volume of the unit cell, B_0 is the bulk modulus, and p_i is the degeneracy of the phonon mode with mode frequency ω_i at the Brillouin zone center. From this equation, a positive and negative mode Grüneisen parameter γ_i, which can be written as $\gamma_i = -\mathrm{d}(\ln \omega_i)/\mathrm{d}(\ln V)$, contributes positively or negatively to the thermal expansion coefficient. It is obvious that all the Raman modes below 100 cm^{-1} give rise to negative slopes vs temperature, implying negative mode Grüneisen parameters since ZrW_2O_8 and HfW_2O_8 have negative thermal expansion coefficients. Therefore, the three lowest phonon modes contribute greatly to the negative thermal expansion of cubic ZrW_2O_8 and HfW_2O_8. As can be seen from Figures 5 and 6, some of the high-frequency stretching modes, particularly the asymmetric stretching modes, give rise also to negative slopes vs temperature and hence contribute also to the negative thermal expansion. This confirms that the correlated motions of transilation and libration with the asymmetric stretching vibrations of the polyhedra are responsible for the negative thermal

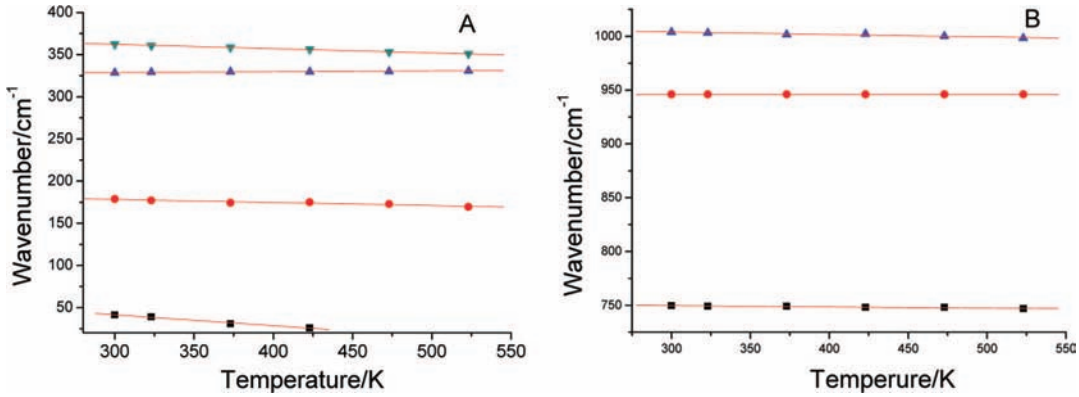

Figure 8. Temperature dependence of the Raman band positions of $ZrMo_2O_8$.

expansion in the low-temperature phase. Above 440 K, some of the correlated motions may be destroyed as evidenced by the disappearance of the coupled librational motion around 40 cm^{-1} with the marked weakening of the out-of-phase asymmetric stretching vibration across the order−disorder phase transition and cause a smaller negative thermal expansion of the β phase.

Figure 7 shows the Raman spectra of trigonal $ZrMo_2O_8$ measured at different temperatures. The lowest Raman mode at 39 cm^{-1} shifts quickly to lower frequencies and outside the detection limit. It is shown that all the Raman mode positions show negative slopes with temperature (see Figure 8A,B). The negative slopes give rise to positive Grüneisen parameters and contribute positively to the thermal expansion in this material. The same has been observed for trigonal $HfMo_2O_8$.

IV. Conclusion

The phonon modes of cubic ZrW_2O_8 and HfW_2O_8, and trigonal $ZrMo_2O_8$ and $HfMo_2O_8$ have been comparatively studied by Raman and THz-TD spectroscopy. The replacement of Zr by Hf atoms hardens all the internal vibrational modes and pushes the lowest asymmetric stretching modes much more to higher energies than the symmetric stretching and the bending modes, resulting in a larger phonon band gap in α-HfW_2O_8 and α-$HfMo_2O_8$. In the cubic ZrW_2O_8 and HfW_2O_8 there appear a number of distinctive low-frequency modes below 150 cm^{-1} in both Raman and terahertz spectra which are attributed to the librational and translational motions of the polyhedra, whereas there appears only one weak Raman mode around 34−39 cm^{-1} in trigonal $ZrMo_2O_8$ and $HfMo_2O_8$, which is IR-inactive and attributed to the interlayer breathing motions driven by van der Waals forces. It is found that the lowest phonon mode at about 40 cm^{-1} disappears accompanied by obvious weakening of the lowest asymmetric stretching mode at about 735 cm^{-1} for ZrW_2O_8 and 757 cm^{-1} for HfW_2O_8 across the order−disorder phase transition temperature. This gives direct evidence of a reduction in the number of QRUMs in the high-temperature phase. The correlated motions of the libration of the WO_4 tetrahedra and the ZrO_6/HfO_6 octahedra with the out-of-phase asymmetric stretching of the two neighboring WO_4 tetrahedra in the low-temperature phase give rise to a large potion of contribution to the NTE in the low-temperature phase. Some of the correlated motions may be destroyed across the order−disorder phase transition and cause a smaller negative thermal expansion of the β phase. All the Raman modes in trigonal $ZrMo_2O_8$ and $HfMo_2O_8$ exhibit positive Grüneisen parameters and hence contribute positively to their thermal expansion. The lack of RUMs in trigonal $ZrMo_2O_8$ and $HfMo_2O_8$, suggesting that the polyhedra in the densely packed layer do not have enough flexibility for librational and translational motions, is the cause of positive thermal expansion in these two materials.

Acknowledgment. The authors acknowledge Dr. Juntao Yang from the Renishaw Beijing office and Dr. Shifeng Liu and Ms. Yumei Pu from the Jobin Yvon Beijing office for their assistance in Raman spectra measurements. We also acknowledge Dr. Z. Y. Zhang in the Shanghai Institute of Applied Physics, Chinese Academy of Sciences and Dr. C. H. Zhang and Mr. J. L. Ma in the Institute of Low Temperature Physics of Nanjing University for the THz-TDS measurements. This work was supported by the National Natural Science Foundation of China (Grant No. 10574113) and the National High Tech. Program of China (Grant No. 2007XX0662).

References and Notes

(1) Mary, T. A.; Evans, J. S. O.; Vogt, T.; Sleight, A. W. *Science* **1996**, *272*, 90.
(2) Evans, J. S. O.; Hu, Z.; Jorgensen, J. D.; Argyriou, D. N.; Short, S.; Sleight, A. W. *Science* **1997**, *275*, 61.
(3) Pryde, A. K. A.; Hammonds, K. D.; Dove, M. T.; Heine, V.; Gale, J. D.; Warren, M. C. *J. Phys.: Condens. Matter* **1996**, *8*, 10973.
(4) Tucker, M. G.; Goodwin, A. L.; Dove, M. T.; Keen, D. A.; Wells, S. A.; Evans, J. S. O. *Phys. Rev. Lett.* **2005**, *95*, 255501.
(5) Mittal, R.; Chaplot, S. L. *Prog. Mater. Sci.* **2006**, *51*, 211.
(6) Ravindran, T. R.; Arora, A. K.; Sairam, T. N. *J. Raman Spectrosc.* **2007**, *38*, 283.
(7) Ding, P.; Liang, E. J.; Jia, Y.; Du, Z. Y. *J. Phys.: Condens. Matter* **2008**, *20*, 275224.
(8) Liang, E. J.; Huo, H. L.; Wang, J. P.; Chao, M. J. *J. Phys. Chem. C* **2008**, *112*, 6577.
(9) Hancock, J. N.; Turpen, C.; Schlesinger, Z.; Kowach, G. R.; Ramirez, A. P. *Phys. Rev. Lett.* **2004**, *93*, 225501.
(10) Tao, J. Z.; Sleight, A. W. *J. Solid State Chem.* **2003**, *173*, 442.
(11) Evans, J. S. O.; Mary, T. A.; Vogt, T.; Subramanian, M. A.; Sleight, A. W. *Chem. Mater.* **1996**, *8*, 2809.
(12) Ernst, G.; Broholm, C.; Kowach, G. R.; Ramirez, A. P. *Nature* **1998**, *396*, 147.
(13) Ramirez, A. P.; Kowach, G. R. *Phys. Rev. Lett.* **1998**, *80*, 4903.
(14) David, W. I. F.; Evans, J. S. O.; Sleight, A. W. *Europhys. Lett.* **1999**, *46*, 661.
(15) Evans, J. S. O.; David, W. I. F.; Sleight, A. W. *Acta Crystallogr., Sect. B: Struct. Sci.* **1999**, *B 55*, 333.
(16) Yamamura, Y.; Nakajima, N.; Tsuji, T.; Iwasa, Y.; Saito, K.; Sorai, M. *Solid State Commun.* **2002**, *121*, 213.
(17) Yamamura, Y.; Nakajima, N.; Tsuji, T.; Koyano, M.; Iwasa, Y.; Katayama, S.; Saito, K.; Sorai, M. *Phys. Rev. B* **2002**, *66*, 014301.
(18) Perottoni, C. A.; da Jornada, J. A. H. *Science* **1998**, *280*, 886.
(19) Ravindran, T. R.; Arora, A. K.; Mary, T. A. *J. Phys.: Condens. Matter* **2001**, *13*, 11573.

(20) Ravindran, T. R.; Arora, A. K.; Mary, T. A. *Phys. Rev. Lett.* **2000**, *34*, 3879.
(21) Ravindran, T. R.; Arora, A. K.; Mary, T. A. *Phys. Rev. B* **2003**, *67*, 064301.
(22) Liang, E. J.; Wang, S. H.; Wu, T. A.; Chao, M. J.; Yuan, B.; Zhang, W. F. *J. Raman Spectrosc.* **2007**, *38*, 1186.
(23) Liang, E. J.; Wu, T. A.; Yuan, B.; Chao, M. J.; Zhang, W. F. *J. Phys. D: Appl. Phys.* **2007**, *40*, 3219.
(24) Liang, E. J.; Wang, J. P.; Xu, E. M.; Du, Z. Y.; Chao, M. J. *J. Raman Spectrosc.* **2008**, *39*, 887.
(25) Arora, A. K.; Sastry, V. S.; Sahu, P.; Mary, T. A. *J. Phys.: Condens. Matter* **2004**, *16*, 1025.
(26) Pereira, A. S.; Perottoni, C. A.; da Jornada, J. A. H. *J. Raman Spectrosc.* **2003**, *34*, 578.
(27) Chen, B.; Muthu, D. V. S.; Liu, Z. X.; Sleight, A. W.; Kruger, M. B. *J. Phys.: Condens. Matter* **2002**, *14*, 13911.
(28) Yamamura, Y.; Nakajima, N.; Tsuji, T. *Phys. Rev. B* **2001**, *64*, 184109.
(29) Yamamura, Y.; Tsuji, T.; Saito, K.; Sorai, M. *J. Chem. Thermodyn.* **2004**, *36*, 525.
(30) Carlson, S.; Andersen, A. M. K. *Phys. Rev. B* **2000**, *61*, 11209.
(31) Andersen, A. M. K.; Carlson, S. *Acta Crystallogr. Sect. B: Struct. Sci.* **2001**, *57*, 20.
(32) Scott, J. F. *J. Chem. Phys.* **1968**, *48*, 874.
(33) Du, Z. Y. Master Thesis, Zhengzhou University, 2008.
(34) Mittal, R.; Chaplot, S. L.; Lalla, N. P.; Mishra, R. K. *J. Appl. Cryst.* **1999**, *32*, 1010.

JP805256D